Temporal surrogates of spatial turbulent statistics: The Taylor hypothesis revisited

Victor S. L'vov, Anna Pomyalov, and Itamar Procaccia
Department of Chemical Physics, The Weizmann Institute of Science, Rehovot 76100, Israel
(Received 10 May 1999)

The Taylor hypothesis, which allows surrogating spatial measurements requiring many experimental probes by time series from one or two probes, is examined on the basis of a simple analytic model of turbulent statistics. The main points are as follows: (i) The Taylor hypothesis introduces *systematic* errors in the evaluation of scaling exponents. (ii) When the mean wind $\overline{V}_0$ is not infinitely larger than the root-mean-square longitudinal turbulent fluctuations v_T, the effective Taylor advection velocity V_{ad} should take the latter into account. (iii) When two or more probes are employed the application of the Taylor hypothesis and the optimal choice of the effective advecting wind V_{ad} need extra care. We present practical considerations for minimizing the errors incurred in experiments using one or two probes. (iv) Analysis of the Taylor hypothesis when different probes experience different mean winds is offered. [S1063-651X(99)14010-8]

PACS number(s): 47.27.−i

I. INTRODUCTION

Decades of research on the statistical aspects of thermodynamic turbulence are based on the Taylor hypothesis [1], which asserts that the fluctuating velocity field measured by a given probe as a function of time; $\boldsymbol{u}(t)$ is the same as the velocity $\boldsymbol{u}(R/\overline{V}_0)$ where $\overline{V}_0$ is the mean velocity and R is the distance to a position ''upstream'' where the velocity is measured at $t=0$. Sixty years after its introduction by Taylor, this time-honored hypothesis remains the only really convenient way to measure experimentally turbulent velocity fluctuations. New techniques were introduced in recent years, but so far did not make a lasting mark on the field. On the other hand, theoretical considerations of the anomalous nature of the statistics of turbulence have made higher and higher demands on the accuracy of experimental measurements, with finer details being asked by experimentalists and theorists alike. In light of these demands it seems necessary to revisit the Taylor hypothesis at this point to assess its consequences regarding the accuracy of measurements of scaling exponents in turbulent media.

Our own motivation to study the consequences of the Taylor hypothesis stems from attempts to develop a deeper understanding of the effects of anisotropy on turbulent statistics [2,3]. In the context of this program it turned out that the interpretation of experimental signals in turbulent systems with shear poses delicate issues that call for careful considerations. In order to expose anisotropic features one needs to analyze data pertaining to at least two probes. In the case of shear each probe may experience a different mean velocity, and velocity differences between such two probes (which are computed using Taylor surrogates) mix spatial and temporal dependencies. The considerations taken to clarify such issues are assisted by the analysis of a simple model of turbulent advection, which sheds light on how to treat systems with shear, but also can be used to improve the understanding of the Taylor hypothesis in systems that are homogeneous and isotropic. It seems, therefore, worthwhile to present the model and its consequence for the benefit of the general turbulence community, which may find it useful for more than one application.

The Taylor hypothesis was studied carefully in the 1950's [4–7], and continues to be the subject of scrutiny to this day [8–10]. Some of the inherent limitations implied by the Taylor hypothesis were pointed out in these studies. Our purpose in this paper is to offer rational choices to minimize the systematic errors that are entailed in the standard experimental procedures. To this aim we need to study the systematic errors, something that can be done only by comparing spatial statistics to temporal statistics. Not being able to do this directly on the basis of the Navier-Stokes equations, we offer a model of turbulent fluctuations advected by a ''wind'' of desired properties, be them homogeneous or not. The model allows us to compute explicitly correlation functions or structure functions that depend on space and time. We can then compare the temporal objects (for fixed spatial positions) with simultaneous objects that depend on varying scales. Having full control on the properties of the wind we can analyze the relative importance of the mean wind versus the rms fluctuations and the consequences of inhomogeneities.

In Sec. II we present the issue, introduce the statistical objects under study, and explain the model that is analyzed in the rest of this paper. The model employs an advecting velocity field $\boldsymbol{V}$ and an independent fluctuating field $\boldsymbol{u}$, which is advected without affecting its statistical properties. The latter are chosen to mimic those of Kolmogorov turbulence. The most important property that affects the accuracy of the Taylor surrogate is the effective decay time of fluctuations of scale R. The ratio of the sweeping time across a scale R and this decay time determines the applicability of the Taylor hypothesis. This is made clear in Sec. II. In Sec. III we explore the consequences of the Taylor hypothesis in the case of one probe measurements. We find that the Taylor method introduces systematic errors in the estimated exponents of the second-order structure function. The reason for this error is simply that the Taylor method improves for small scales, where the decay time is always much longer than the sweeping time. Accordingly, there is a systematic improvement of the estimate via surrogates as the relevant length scale decreases. This appears as an apparent ''expo-

nent'' in log-log plots. Nevertheless, we argue that the systematic errors for the isotropic part of the second-order structure function are quite small for realistic choices of the parameters, of the order of 0.01 in the measured exponents. In the same section we discuss the relative contribution of the mean wind and the rms fluctuations to the ''effective'' advecting wind $V_{\rm ad}$ employed in the Taylor hypothesis. We find that the method works even in the absence of mean wind (which has been noticed before, for example, in turbulent convection [8] and in a swirling flow [9]). In general, both contribute to the effective wind, with a parameter of relative importance [denoted b below, see Eq. (47)]. We find that the optimal value of b is larger than anticipated.

In Sec. IV we solve the model in the case of linear shear. The first question analyzed is what is the effective wind that should be taken in surrogating data that stem from two probes that experience different mean winds. We show that for linear shear the answer is simple, i.e., the mean of the mean winds of the two probes. Next we solved the model, and found the corrections to the structure functions due to the existence of the shear. In the language of Ref. [3] this is a $j=2$ anisotropic contribution where j refers to the index of the irreducible representation of the SO(3) symmetry group. The scaling exponent associated with this contribution is 4/3 in the K41 framework, in agreement with measurements and earlier theoretical considerations [12,13]. Last, we assessed the performance of the Taylor method for this contribution and concluded that it is significantly worse than in the isotropic counterpart. The typical errors in estimating the exponent can be as high as 0.1. Section V offers a summary and a discussion. In particular, we present arguments as to which aspects of our conclusions are relatively model independent.

II. THE MODEL

A. Preliminaries

In statistical turbulence one is interested in the statistical properties of the turbulent velocity field $\boldsymbol{u}(\boldsymbol{r},t)$ where $(\boldsymbol{r},t)$ is a space-time point in the laboratory frame (so-called Eulerian velocity). In this paper we will focus on the properties of the second-order space-time correlation function of velocity differences:

$$F^{\alpha\beta}(\boldsymbol{R},t)\equiv\langle[u^{\alpha}(0,t_0)-u^{\alpha}(\boldsymbol{R},t_0+t)]\times[u^{\beta}(0,t_0)-u^{\beta}(\boldsymbol{R},t_0+t)]\rangle, \tag{1}$$

where angular brackets denote averaging with respect to t_0. In this definition and throughout the paper we assume that the turbulence is *stationary* in the sense that the statistical ensemble is time independent. We do not assume space homogeneity or isotropy. For $t=0$ the correlation function $F^{\alpha\beta}(\boldsymbol{R},t)$ turns into the commonly used second-order structure function $S^{\alpha\beta}(\boldsymbol{R})$:

$$S^{\alpha\beta}(\boldsymbol{R})\equiv F^{\alpha\beta}\quad(\boldsymbol{R},t=0). \tag{2}$$

For $\boldsymbol{R}=0$ we have the time-dependent object, which is usually measured in single probe experiments:

$$T^{\alpha\beta}(t)\equiv F^{\alpha\beta}\quad(\boldsymbol{R}=0,t). \tag{3}$$

The Taylor hypothesis is based on the idea that when the mean wind $\overline{\boldsymbol{V}}_0$ is very high, the turbulent field is advected by a given probe as if frozen, having hardly any time to relax while being recorded by the probe. Disregarding the relaxation of turbulent eddies of size R, the hypothesis implies that

$$S^{\alpha\beta}(\boldsymbol{R}=t\overline{\boldsymbol{V}}_0)=T^{\alpha\beta}(t), \tag{4}$$

Obviously, the validity of this hypothesis depends on the ratio of two times scales. The first is the advection time $R/\overline{V}_0$ that it takes to translate structures of size R by the probe. The second is the lifetime $\tau(R)$, which describes the typical decay time of turbulent structures of size R. In the limit $R/[\overline{V}_0\tau(R)]\to 0$ the Taylor hypothesis becomes valid. The typical time scale $\tau(R)$ is inherent to the dynamics of turbulent flows, and is quite independent of the mean wind, which can be eliminated by changing the coordinates to a comoving frame. Up to a factor of order unity the lifetime can be estimated as the turnover time $R/\sqrt{S(R)}$ where $S(R)\equiv S_{\alpha\alpha}(R)$. With this estimate the Taylor hypothesis is expected to be valid when $\sqrt{S(R)}/\overline{V}_0\to 0$. In the sequel we denote the ratio of these two time scales by $z(R)$. Clearly, in turbulence $z(R)$ increases with R, and for R of the order of the outer scale of turbulence it is largest. It is thus sufficient to have very small $z(L)$ to ensure the validity of the Taylor hypothesis for all $r<L$.

In typical experimental conditions like atmospheric turbulence, $z(L)$ is of the order of 0.2–0.5 [10,11]. [Note that in most experimental papers only the longitudinal component of the structure function is available; in isotropic turbulence this is smaller than $S(R)$ by a factor of about 3.] Accordingly, the Taylor hypothesis needs careful scrutiny. Moreover, almost all experiments are forced by anisotropic and inhomogeneous agents, and the ''mean'' velocity depends on the position. When more than one probe is used one needs to decide how to choose $\overline{V}_0$ in Eq. (4). To allow us to answer such questions rationally we study the following model.

B. Basic model

1. Equation of motion

Consider a model turbulent velocity field $\boldsymbol{u}(\boldsymbol{r},t)$ which in $(\boldsymbol{k},\omega)$ representation is defined as

$$\tilde{\boldsymbol{u}}(\boldsymbol{k},\omega)=\int d\boldsymbol{r}\exp[-i(\boldsymbol{r}\cdot\boldsymbol{k}+\omega t)]\boldsymbol{u}(\boldsymbol{r},t). \tag{5}$$

We propose the following model dynamics for $\tilde{\boldsymbol{u}}(\boldsymbol{k},\omega)$:

$$[\omega+\boldsymbol{k}\cdot\boldsymbol{V}_0+i\gamma(k)]\tilde{u}^{\alpha}(\boldsymbol{k},\omega)+\int\frac{d\boldsymbol{k}'\,d\boldsymbol{k}''}{8\pi^3}\times\Gamma^{\alpha\beta\gamma}_{\boldsymbol{k}}V_s^{\beta}(\boldsymbol{k}')\tilde{u}^{\gamma}(\boldsymbol{k}'',\omega)\,\delta(\boldsymbol{k}-\boldsymbol{k}'-\boldsymbol{k}'')=\tilde{f}^{\alpha}(\boldsymbol{k},\omega), \tag{6}$$

$$i\boldsymbol{k}\cdot\tilde{\boldsymbol{u}}(\boldsymbol{k},\omega)=0, \tag{7}$$

where $\Gamma_{\boldsymbol{k}}^{\alpha\beta\gamma}$ is the exact nonlinear vertex that stems from the Navier-Stokes equations:

$$\Gamma_{\boldsymbol{k}}^{\alpha\beta\gamma}=k_\beta P^{\alpha\gamma}(\boldsymbol{k})+k_\gamma P^{\alpha\beta}(\boldsymbol{k}). \tag{8}$$

Here $P^{\alpha\beta}(\boldsymbol{k})$ is the transverse projection operator

$$P^{\alpha\beta}(\boldsymbol{k})=\delta_{\alpha\beta}-\frac{k_\alpha k_\beta}{k^2} \tag{9}$$

and $\delta_{\alpha\beta}$ is the Kronecker symbol. This dynamics represents ''passive vector advection'' in which the ''turbulent'' field $\tilde{\boldsymbol{u}}(\boldsymbol{k},\omega)$ is advected by a statistically independent stationary field $\boldsymbol{V}(\boldsymbol{k})$. In its turn, the wind $\boldsymbol{V}(\boldsymbol{k})$ consist of homogeneous $\boldsymbol{V}_0$ and space dependent $\boldsymbol{V}_s(\boldsymbol{k})$ parts:

$$\boldsymbol{V}(\boldsymbol{k})=(2\pi)^3\delta(\boldsymbol{k})\boldsymbol{V}_0+\boldsymbol{V}_s(\boldsymbol{k}). \tag{10}$$

The homogeneous part $\boldsymbol{V}_0$ appears in Eq. (6) as a Doppler shift to ω. The inverse decay time $\gamma(k)$ represents the eddy viscosity, which mimics the effects of the nonlinear terms in Navier-Stokes dynamics on the energy loss from a given wave number. The forcing term $\boldsymbol{f}(\boldsymbol{k},\omega)$ represents that energy gain.

2. Statistical description

Correlations in $(\boldsymbol{k},\omega)$ *and* $(\boldsymbol{k},t)$ *representation*. Introduce the correlation function of the velocity field $\tilde{\boldsymbol{u}}(\boldsymbol{k},\omega)$ as follows:

$$\langle\tilde{u}^\alpha(\boldsymbol{k},\omega)\tilde{u}^{*\beta}(\boldsymbol{k}',\omega')\rangle\equiv 2\pi\delta(\omega-\omega')\tilde{\Phi}^{\alpha\beta}(\boldsymbol{k},\boldsymbol{k}',\omega). \tag{11}$$

For space-homogeneous ensembles (in our case, in the absence of a shear) $\tilde{\Phi}^{\alpha\beta}(\boldsymbol{k},\boldsymbol{k}',\omega)$ is diagonal in $\boldsymbol{k}$:

$$\tilde{\Phi}^{\alpha\beta}(\boldsymbol{k},\boldsymbol{k}',\omega)=(2\pi)^3\delta(\boldsymbol{k}-\boldsymbol{k}')\tilde{\Phi}^{\alpha\beta}(\boldsymbol{k},\omega). \tag{12}$$

Note that in order to avoid the proliferation of symbols we used the same notation for the two functions $\tilde{\Phi}^{\alpha\beta}(\boldsymbol{k},\boldsymbol{k}',\omega)$ and $\tilde{\Phi}^{\alpha\beta}(\boldsymbol{k},\omega)$. The same two functions in $\boldsymbol{k},t$ representations are distinguished by a ''hat'' symbol:

$$\hat{\Phi}^{\alpha\beta}(\boldsymbol{k},\boldsymbol{k}',t)=\int\frac{d\omega}{2\pi}\,\tilde{\Phi}^{\alpha\beta}(\boldsymbol{k},\boldsymbol{k}',\omega)\exp(i\omega t), \tag{13}$$

$$\hat{\Phi}^{\alpha\beta}(\boldsymbol{k},t)=\int\frac{d\omega}{2\pi}\,\tilde{\Phi}^{\alpha\beta}(\boldsymbol{k},\omega)\exp(i\omega t).$$

The time independent functions $\hat{\Phi}^{\alpha\beta}(\boldsymbol{k},\boldsymbol{k}',t=0)$ and $\hat{\Phi}^{\alpha\beta}(\boldsymbol{k},t=0)$ will remain undecorated:

$$\Phi^{\alpha\beta}(\boldsymbol{k},\boldsymbol{k}')\equiv\hat{\Phi}^{\alpha\beta}(\boldsymbol{k},\boldsymbol{k}',0),\quad \Phi^{\alpha\beta}(\boldsymbol{k})\equiv\hat{\Phi}^{\alpha\beta}(\boldsymbol{k},0). \tag{14}$$

Correlation functions in $(\boldsymbol{r},t)$ *representation.* Introduce correlation functions of the velocity filed $\boldsymbol{u}(\boldsymbol{r},t)$ as follows:

$$\langle u^\alpha(\boldsymbol{r},t)u^\beta(\boldsymbol{r}',t')\rangle\equiv\mathcal{F}^{\alpha\beta}(\boldsymbol{r},\boldsymbol{r}',t-t'), \tag{15}$$

where stationarity in time is assumed. In space homogeneous ensembles $\mathcal{F}^{\alpha\beta}(\boldsymbol{r},\boldsymbol{r}',t)$ depends on the difference $\boldsymbol{R}=\boldsymbol{r}-\boldsymbol{r}'$ only. We will again use an economic notation and employ the symbol $\mathcal{F}^{\alpha\beta}$ also for the space homogeneous case:

$$\mathcal{F}^{\alpha\beta}(\boldsymbol{r},\boldsymbol{r}',t)\Rightarrow\mathcal{F}^{\alpha\beta}(\boldsymbol{R},t). \tag{16}$$

These two functions are related to the corresponding correlation functions in $\boldsymbol{k},t$ representation by

$$\mathcal{F}^{\alpha\beta}(\boldsymbol{r},\boldsymbol{r}',t)=\int\frac{d\boldsymbol{k}d\boldsymbol{k}'}{(2\pi)^6}\,\hat{\Phi}^{\alpha\beta}(\boldsymbol{k},\boldsymbol{k}',t)\exp[i(\boldsymbol{k}\cdot\boldsymbol{r}-\boldsymbol{k}'\cdot\boldsymbol{r}')], \tag{17}$$

$$\mathcal{F}^{\alpha\beta}(\boldsymbol{R},t)=\int\frac{d\boldsymbol{k}}{(2\pi)^3}\,\hat{\Phi}^{\alpha\beta}(\boldsymbol{k},t)\exp(i\boldsymbol{k}\cdot\boldsymbol{R}). \tag{18}$$

On the other hand the function $F^{\alpha\beta}$ of Eq. (1) is computed as

$$F^{\alpha\beta}(\boldsymbol{R},t)=2\int\frac{d\boldsymbol{k}}{(2\pi)^3}\,\hat{\Phi}^{\alpha\beta}(\boldsymbol{k},t)[1-\exp(i\boldsymbol{k}\cdot\boldsymbol{R})]. \tag{19}$$

3. Choice of parameters in the model

The advecting wind. In our thinking we are inspired by experiments in the atmospheric boundary layer in which the advecting wind may be considered as consisting of three parts. The first component can be taken as a space-time independent mean wind $\overline{\boldsymbol{V}_0}$, which is constant for our ensemble. The second component is a space-time independent part that is constant on the time scale of a typical experiment (minutes), but changes from one experimental realization in the ensemble to another. We denote it as $\boldsymbol{V}_T$. We will assume that it fluctuates randomly between different experimental realizations of the ensemble. The third part is an explicitly space dependent part of the mean wind denoted as above $\boldsymbol{V}_s(\boldsymbol{r})$. Note that again we avoid proliferating the symbols, and we use the same symbol $\boldsymbol{V}_s$ in $\boldsymbol{k}$ and $\boldsymbol{r}$ representation. Accordingly, we can write

$$\boldsymbol{V}_0=\overline{\boldsymbol{V}_0}+\boldsymbol{V}_T,\quad \overline{\boldsymbol{V}_T}=0. \tag{20}$$

Since $\boldsymbol{V}_T$ is considered as a random variable we need to specify its probability distribution function. This is denoted $\mathcal{P}(\boldsymbol{V}_T)$, and overlines as in Eq. (20) denote averages with respect to this distribution. We will solve the correlation functions $\tilde{\boldsymbol{\Phi}}(\boldsymbol{k},\omega)$ for each realization of $\boldsymbol{V}_0$ and average the result with respect to $\mathcal{P}(\boldsymbol{V}_T)$. The amplitude of the mean-square fluctuations of $\boldsymbol{V}_T$ are chosen such that

$$\overline{V_{T^2}}=3v_T^2, \tag{21}$$

where v_T^2 is a mean-square fluctuation of the longitudinal turbulent velocity.

The inhomogeneous part of the wind will not be random. To simplify the analytical calculations the space dependent $\boldsymbol{V}_s(\boldsymbol{r})$ is chosen as a sinusoidal profile,

$$\boldsymbol{V}_s(\boldsymbol{r})=\boldsymbol{n}V_s\sin(\boldsymbol{q}\cdot\boldsymbol{r}),\quad \boldsymbol{q}=q\boldsymbol{m}, \tag{22}$$

where $\boldsymbol{m}$ and $\boldsymbol{n}$ are unit vectors in the vertical and horizontal directions respectively. The horizontal direction is the direction of the mean wind: $\overline{\boldsymbol{V}}_0 = \boldsymbol{n}\overline{V}_0$. In $\boldsymbol{k}$ representation Eq. (22) reads:

$$\boldsymbol{V}_s(\boldsymbol{k}) = \frac{(2\pi)^3}{2} V_s \boldsymbol{n}[\delta(\boldsymbol{k}-\boldsymbol{q}) - \delta(\boldsymbol{k}+\boldsymbol{q})]. \tag{23}$$

Note that sinusoidal profile (22) has nothing to do with the logarithmic profile in real boundary layers. For small $\boldsymbol{q}$ it mimics locally a linear shear.

The lifetime of eddies. A good model for $\gamma(k)$ in Eq. (6) is provided by the Kolmogorov 41 model of turbulence in which the lifetime $1/\gamma(k)$ is defined as the turnover time up to an unknown dimensionless (universal) factor C:

$$\gamma(k) = C\frac{v_T}{L}(kL)^{2/3}. \tag{24}$$

Here L is the integral scale of turbulence and v_T^2 is the mean square longitudinal velocity, which in isotropic conditions equals

$$v_T^2 = \tfrac{1}{3}\langle |\boldsymbol{u}(\boldsymbol{r},t)|^2\rangle. \tag{25}$$

The forcing term $\boldsymbol{f}(\boldsymbol{k},\omega)$. In this paper we are interested in second-order turbulent statistics. Therefore, it is sufficient to model $\boldsymbol{f}(\boldsymbol{k},\omega)$ as Gaussian white noise:

$$\langle \tilde{f}^{\alpha}(\boldsymbol{k},\omega)\tilde{f}^{*\beta}(\boldsymbol{k}',\omega')\rangle = (2\pi)^4 \delta(\omega-\omega')\,\delta(\boldsymbol{k}-\boldsymbol{k}')D^{\alpha\beta}(\boldsymbol{k}). \tag{26}$$

Since our model is linear in the turbulent velocity $\tilde{\boldsymbol{u}}$, there is a simple relation between the intensity of the noise $D^{\alpha\beta}(\boldsymbol{k})$ and the simultaneous correlation function of the turbulent velocity $\Phi_0^{\alpha\beta}(\boldsymbol{k})$, where the subscript ''0'' denotes the absence of the shear flow. The relation is [and cf. Eq. (34) below]

$$D^{\alpha\beta}(\boldsymbol{k}) = 2\gamma(k)\Phi_0^{\alpha\beta}(\boldsymbol{k}). \tag{27}$$

The tensorial structure of $\Phi_0^{\alpha\beta}(\boldsymbol{k})$ is determined by the incompressibility condition

$$\Phi_0^{\alpha\beta}(\boldsymbol{k}) = P^{\alpha\beta}(\boldsymbol{k})\Phi_0(k), \tag{28}$$

and what remains is to select the scalar function $\Phi_0(k)$. To do this we refer again to the K41 model and choose

$$\Phi_0(\boldsymbol{k}) = \frac{\phi}{[(kL)^2+1]^{11/6}}, \tag{29}$$

with some amplitude ϕ. In the inertial interval, i.e., for $kL \gg 1$. Equation (29) agrees with the standard Kolmogorov scaling, $\Phi_0(\boldsymbol{k}) \propto k^{-11/3}$. The form of Eq. (29) is not unique, and other forms exhibiting different crossovers between power law scaling and saturation are equally acceptable. For example instead of Eq. (29) we may also choose

$$\Phi_0(\boldsymbol{k}) = \frac{\phi}{(kL)^{11/3}+1}. \tag{30}$$

We will show below that our conclusions are only weakly affected by the precise choice of crossover behavior. This completes the setup of the model.

III. SOLUTIONS OF THE MODEL WITHOUT SHEAR

A. Homogeneous advection

First we analyze the situation without shear, $V_s = 0$. The resulting velocity field $\tilde{\boldsymbol{u}}_0(\boldsymbol{k},\omega)$ and all the other objects will be denoted by a subscript '' $_0$ '' to remind us that $V_s = 0$. In this case the integral in Eq. (6) vanishes and the solution for $\tilde{\boldsymbol{u}}_0(\boldsymbol{k},\omega)$ immediately follows:

$$\tilde{\boldsymbol{u}}_0(\boldsymbol{k},\omega) = G_0(\boldsymbol{k},\omega)\tilde{\boldsymbol{f}}(\boldsymbol{k},\omega), \tag{31}$$

$$G_0(\boldsymbol{k},\omega) \equiv \frac{1}{\omega + \boldsymbol{k}\cdot\boldsymbol{V}_0 + i\gamma(k)}. \tag{32}$$

One sees that the effect of the space homogeneous part of the advecting velocity field amounts to a Doppler shift only. Using definitions (11), (12), and (26) one has

$$\tilde{\Phi}_0^{\alpha\beta}(\boldsymbol{k},\omega) = D^{\alpha\beta}(\boldsymbol{k})|G_0(\boldsymbol{k},\omega)|^2. \tag{33}$$

The equation for the simultaneous correlation function follows from Eq. (13):

$$\Phi_0^{\alpha\beta}(\boldsymbol{k}) = \int \frac{d\omega}{2\pi}\,\tilde{\Phi}_0^{\alpha\beta}(\boldsymbol{k},\omega) = \frac{D^{\alpha\beta}(\boldsymbol{k})}{2\gamma(k)}. \tag{34}$$

This is consistent with Eq. (27). The correlation function in $(\boldsymbol{k},t)$ representation is computed straightforwardly,

$$\hat{\Phi}_0^{\alpha\beta}(\boldsymbol{k},t) = \int \frac{d\omega}{2\pi}\,\tilde{\Phi}_0^{\alpha\beta}(\boldsymbol{k},\omega)\exp(i\omega\tau) \tag{35}$$

$$= \Phi_0^{\alpha\beta}(\boldsymbol{k})\exp[i\boldsymbol{k}\cdot\boldsymbol{V}_0 t - \gamma(k)t].$$

At this point we recall that $\boldsymbol{V}_0$ contains a term that is stochastic, i.e., $\boldsymbol{V}_T$, see Eq. (20). The averaging of Eq. (35) yields

$$\hat{\Phi}_0^{\alpha\beta}(\boldsymbol{k},t) = \Phi_0^{\alpha\beta}(\boldsymbol{k})\exp\{i\boldsymbol{k}\cdot\overline{\boldsymbol{V}}_0 t - \gamma(k)t - 2(v_T k t)^2\}. \tag{36}$$

The first term in the exponent stems from the advection by the mean wind $\overline{\boldsymbol{V}}_0$. The second one is the correlation decay due to the finite lifetime of the fluctuations. The last term in the exponent describes the effect of decorrelation due to the random sweeping by the random component $\boldsymbol{V}_T$.

Using Eq. (19) we compute

$$F_0^{\alpha\beta}(\boldsymbol{R},t) = \int \frac{d\boldsymbol{k}}{4\pi^3}\Phi_0^{\alpha\beta}(\boldsymbol{k})\{1 - \exp[-2(v_T k t)^2 - \gamma(k)|t|]$$

$$\times\cos(\boldsymbol{k}\cdot\boldsymbol{R} - \boldsymbol{k}\cdot\overline{\boldsymbol{V}}_0 t)\}. \tag{37}$$

The structure function $S_0^{\alpha\beta}(R)$ is obtained from Eq. (37) by substituting $t = 0$:

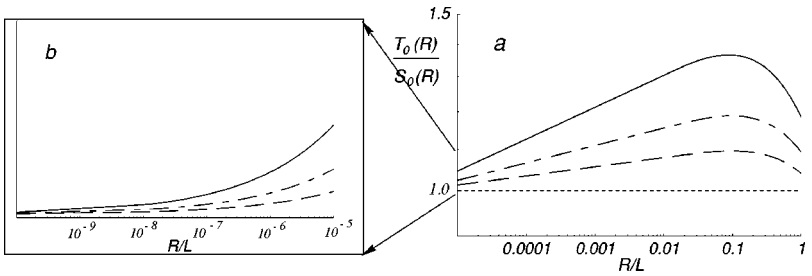

FIG. 1. A log-log plot of the ratio of $T_0(R/V_{ad})/S_0(R)$ vs R/L for three values of C, $C=0.25$ (dashed line), 0.5 (dot-dashed line) and 1 (solid line), and $\overline{V}_0=0$ $(q\to\infty)$. Panel (a) corresponds to R/L between 1 and 10^{-5}, the blowup in panel (b) shows the next five decades of R/L between 10^{-5} and 10^{-10}.

$$S_0^{\alpha\beta}(\boldsymbol{R})=\int \frac{d\boldsymbol{k}}{4\pi^3}\Phi_0^{\alpha\beta}(\boldsymbol{k})\{1-\cos(\boldsymbol{k}\cdot\boldsymbol{R})\}. \tag{38}$$

On the other hand $T_0^{\alpha\beta}(t)$ is obtained by putting $r=0$:

$$T_0^{\alpha\beta}(t)=\int \frac{d\boldsymbol{k}}{4\pi^3}\Phi_0^{\alpha\beta}(\boldsymbol{k})\{1-\exp[-2(v_T kt)^2-\gamma(k)|t|] \times\cos(\boldsymbol{k}\cdot\overline{\boldsymbol{V}}_0 t)\}. \tag{39}$$

We can compare the two expressions for any of the tensor components. Since we are interested in exponents, it is natural to consider first the trace. In order to assess the sensitivity of our results to the tensorial structure we will consider then the longitudinal structure function:

$$S_0(R)=\sum_{\alpha,\beta} S_0^{\alpha\beta}(\boldsymbol{R}),\quad T_0(t)=\sum_{\alpha,\beta} T_0^{\alpha\beta}(t), \tag{40}$$

$$S_0^{//}(\boldsymbol{R})=\sum_{\alpha,\beta} S_0^{\alpha\beta}(\boldsymbol{R})\frac{R_\alpha R_\beta}{R^2},$$

$$T_0^{//}(t)=\sum_{\alpha,\beta} T_0^{\alpha\beta}(t)\frac{\overline{V}_0^\alpha\overline{V}_0^\beta}{\overline{V}_0^2}.$$

Computing the trace, longitudinal projections and performing the angular integrations we end up with

$$S_0(\boldsymbol{R})=\int_0^\infty\frac{k^2dk}{\pi^2}\Phi_0(k)\{1-\Psi_0(kr)\}, \tag{41}$$

$$S_0^{//}(\boldsymbol{R})=\int_0^\infty\frac{k^2dk}{3\pi^2}\Phi_0(k)\{1-\Psi_0^{//}(kr)\},$$

$$T_0(t)=\int_0^\infty\frac{k^2dk}{\pi^2}\Phi_0(k) \times\{1-\Psi_0(k\overline{V}_0 t)\exp[-2(v_T kt)^2-\gamma(k)|t|]\}, \tag{42}$$

$$T_0^{//}(t)=\int_0^\infty\frac{k^2dk}{3\pi^2}\Phi_0(k) \times\{1-\Psi_0^{//}(k\overline{V}_0 t)\exp[-2(v_T kt)^2-\gamma(k)|t|]\}, \tag{43}$$

$$\Psi_0(x)=\frac{\sin(x)}{x},\quad \Psi_0^{//}(x)=3\left[\frac{\sin(x)}{x^3}-\frac{\cos(x)}{x^2}\right]. \tag{44}$$

Equation (25) allows one to express v_T in terms of $\Phi_0(k)$:

$$v_T^2=\frac{1}{3}\langle|\boldsymbol{u}_0(\boldsymbol{r})|^2\rangle=\int\frac{d\boldsymbol{k}}{12\pi^3}\Phi_0(k)=\int_0^\infty\frac{k^2dk}{3\pi^2}\Phi_0(k). \tag{45}$$

B. Assessment of the Taylor hypothesis for homogeneous advection

The comparison between $S_0(\boldsymbol{R})$ and $T_0(t)$ is determined by the two free coefficients in this model, C of Eq. (24) and

$$q\equiv v_T/\overline{V}_0. \tag{46}$$

In comparing the two functions we have freedom in defining the effective advecting mean wind V_{ad}. In the Taylor hypothesis $V_{ad}=\overline{V}_0$, and one is supposed to identify $T_0(t=|\boldsymbol{R}/\overline{V}_0|)$ with $S_0(\boldsymbol{R})$. In some applications, when $\overline{V}_0=0$ the Taylor hypothesis has been used [8] with $V_{ad}=v_T$. In our comparison we find it advantageous to employ an interpolation formula

$$V_{ad}=\sqrt{\overline{V}_0^2+(bv_T)^2}, \tag{47}$$

with b chosen to minimize the difference between the two functions, Eqs. (41) and (42). Of course, for one probe measurement the apparent *scaling exponent* is always independent of the choice of the effective advective wind and of the parameter b in particular. For two or several probe measurements, when we face a mixture of temporal and spatial contributions to the total separation, the choice of V_{ad} and of the parameter b become important as discussed below.

In Fig. 1 we present a log-log plot of the ratio of $T_0(R/V_{ad})/S_0(R)$ vs R/L for three values of C,$C=0.25$,0.5, and 1, and $\overline{V}_0=0$ $(q\to\infty)$. If the Taylor hypothesis were exact, this ratio would have been unity for all R. We find that in the limit $R/L\to0$ the ratio of these two functions goes to a constant, which depends on the choice of b in Eq. (47). This reflects the correctness of the Taylor hypothesis for $R/L\to0$, which follows from the fact that the sweeping time R/V_{ad} is negligible compared to the lifetime $\propto R^{2/3}$. The relation between the units of distance and the units of time needs to be determined. We fix the parameter b by the requirement that $T_0(R/V_{ad})$ should equal $S_0(R)$ when $R/L\to0$. We found that the effective wind may be approximated by Eq. (47) with

$b\approx 3.1$ for the modulo structure function $S_0(R)$.

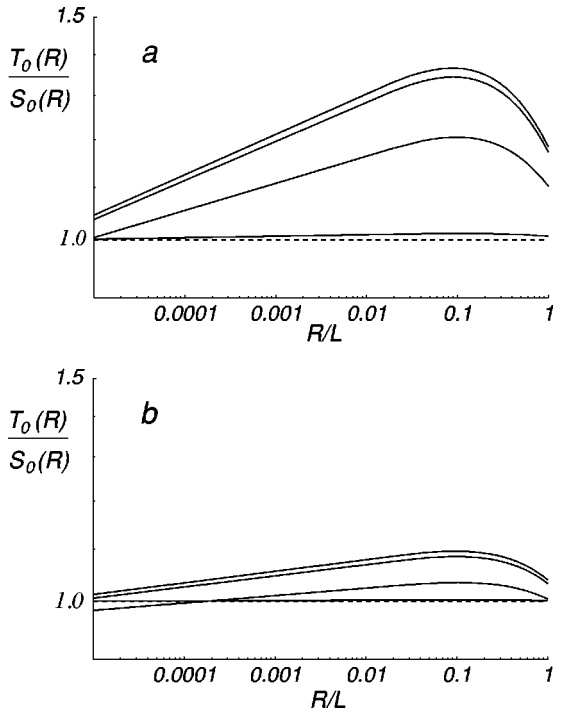

FIG. 2. A log-log plot of the ratio of $T_0(R/V_{ad})/S_0(R)$ vs R/L for $C=1$ [Panel (a)] and $C=0.25$ [Panels (b)]. Different solid lines correspond to values $q=10$, upper line; $q=1$,0.25 from top to bottom; and $q=0.01$, the bottom solid line. Dashed line shows the limit $q\to 0$, when the Taylor hypothesis is exact.

This fixing of the units will be of crucial importance when we discuss two-probe measurements below.

We see that the ratio $T_0(R/V_{ad})/S_0(R)$ does not scale with R when many decades of R are available. In most experiments the range of available R is much smaller, and *apparent* scaling will result. To demonstrate this we present in Fig. 1(b) log-log plots of the ratio of $T_0(R/V_{ad})/S_0(R)$ vs R/L for the same values of C but for R values spanning only the last five decades of scales. Clearly, the plots seem linear over at least four decades.

In Fig. 2 we show log-log plots of the same ratio, for $c=0.25$ and $C=1$, and for values of q ranging from 0.01 to 10. We see that for $C=1$ when the mean wind is four times larger than v_T we have up to 20% deviations in the magnitude of $T_0(R/V_{ad})/S_0(R)$ from unity. For q large (the graphs almost saturate for $q=10$) the deviations reach the apparent scaling exponent the almost linear log-log plots can easily deceive even an experienced researcher to conclude that the value of ζ is larger than what could be measured from spatial differences via $S_0(R)$. This finding is in agreement with the conclusion of Sreenivasan's group [14,15] who studied this issue experimentally. Within our model we can see that the apparent scaling exponent depends on the parameter C, which govern the decay time of fluctuations, cf. Eq. (24). For $C=1$ we find an increase in the apparent exponent ζ_2 between 0.01 and 0.03 depending on the value of d, varying from 0.1 to ∞. For $C=0.25$ the increase is depressed by a factor of 3. The lesson is that for experimental applications it is very advisable to achieve a good estimate of the inherent decay time of fluctuations of size R.

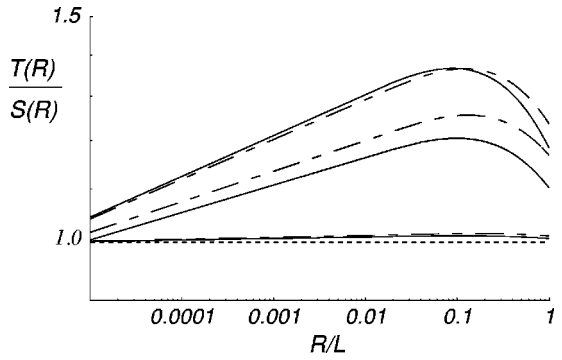

FIG. 3. A log-log plot of the ratio of $T_0(R/V_{ad})/S_0(R)$ vs R/L (solid lines) and $T^{///}(R/V_{ad})/S_2^{///}(R)$ (dot-dashed lines) vs R/L for $C=1$. Different lines correspond to (from the top to the bottom) $q=\infty$, $q=0.25$, and $q=0.01$.

In order to check how our results depend on the tensorial structure of the correlation functions we repeated the same comparisons for the longitudinal structure functions $S_0^{///}$ and $T_0^{///}$. We found that the unit fixing parameter b in this case differs from the previous one:

$$b\approx 4.2 \text{ for the longitudinal structure function } S_0^{///}(R).$$

In order to demonstrate that apparent corrections to the scaling exponents are similar for different tensorial components we plotted in Fig. 3 the ratios $T_0(R/V_{ad})/S_0(R)$ (solid lines) and $T_0^{///}(R/V_{ad})/S_0^{///}(R)$ (dot-dashed lines) vs R for several values of C and q. One sees that with the proper choice of b, these ratios practically coincide.

The conclusions of this part of the analysis are as follows: (i) The best values of b are significantly larger than the naive choice $\sqrt{3}$. They depend on the choice of tensorial components of the correlation functions. (ii) The parameter C, which determines the lifetime $\gamma(k)$, should be known in order to assess the systematic errors involved in the Taylor hypothesis.

IV. THE CASE OF SHEAR

A. Solution for linear shear

In this section we seek the first-order corrections to the second-order correlation functions S and T, which are caused by the existence of a small shear $U_s \ll \overline{V_0}$. To this aim we split the velocity field into homogeneous and shear-induced contributions:

$$\tilde{\boldsymbol{u}}(\boldsymbol{k},\omega)=\tilde{\boldsymbol{u}}_0(\boldsymbol{k},\omega)+\tilde{\boldsymbol{u}}_s(\boldsymbol{k},\omega), \tag{48}$$

where as before, $\tilde{\boldsymbol{u}}_0(\boldsymbol{k},\omega)$ is the solution with zero shear given by Eq. (31), and $\tilde{\boldsymbol{u}}_s(\boldsymbol{k},\omega)$ is induced by the shear V_s. To find $\tilde{\boldsymbol{u}}_s$, we use Eq. (6) with $\tilde{\boldsymbol{u}}(\boldsymbol{k},\omega)$ from Eq. (48), $\tilde{\boldsymbol{u}}_0(\boldsymbol{k},\omega)$ from Eq. (31), and $\boldsymbol{V}(\boldsymbol{k})$ from Eqs. (10) and (23) to get

$$\tilde{\boldsymbol{u}}_s(\boldsymbol{k},\omega)=\tilde{\boldsymbol{u}}_{\boldsymbol{q}}(\boldsymbol{k},\omega)-\tilde{\boldsymbol{u}}_{-\boldsymbol{q}}(\boldsymbol{k},\omega), \tag{49}$$

$$\tilde{\boldsymbol{u}}^{\alpha}_{\pm\boldsymbol{q}}(\boldsymbol{k},\omega)=\tfrac{1}{2}V_{\mathrm{s}}P^{\alpha\beta}(\boldsymbol{k})[(\boldsymbol{k}\cdot\boldsymbol{n})\delta_{\beta\gamma}+n^{\beta}q^{\gamma}] \times G_0(\boldsymbol{k},\omega)G_0(\boldsymbol{k}\mp\boldsymbol{q},\omega)\tilde{f}^{\gamma}(\boldsymbol{k}\mp\boldsymbol{q}). \quad (50)$$

Having defined the velocity field we return to the correlation function Eq. (11) and split $\tilde{\Phi}^{\alpha\beta}(\boldsymbol{k},\boldsymbol{k}',\omega)$ into isotropic and anisotropic, shear-induced, contributions:

$$\tilde{\boldsymbol{\Phi}}^{\alpha\beta}(\boldsymbol{k},\boldsymbol{k}',\omega)=(2\pi)^3\delta(\boldsymbol{k}-\boldsymbol{k}')\tilde{\boldsymbol{\Phi}}^{\alpha\beta}_0(\boldsymbol{k},\omega)+\tilde{\boldsymbol{\Phi}}^{\alpha\beta}_{\mathrm{s}}(\boldsymbol{k},\boldsymbol{k}',\omega). \quad (51)$$

Here $\tilde{\Phi}^{\alpha\beta}_0(\boldsymbol{k},\omega)$ is given by Eq. (33). According to Eqs. (48) and (50) and definition (11) the equation for $\tilde{\boldsymbol{\Phi}}^{\alpha\beta}_{\mathrm{s}}(\boldsymbol{k},\boldsymbol{k}',\omega)$ may be presented as a sum:

$$\tilde{\boldsymbol{\Phi}}^{\alpha\beta}_{\mathrm{s}}(\boldsymbol{k},\boldsymbol{k}',\omega)=\tilde{\boldsymbol{\Phi}}^{\alpha\beta}_{\boldsymbol{q}}(\boldsymbol{k},\boldsymbol{k}',\omega)-\tilde{\boldsymbol{\Phi}}^{\alpha\beta}_{-\boldsymbol{q}}(\boldsymbol{k},\boldsymbol{k}',\omega) +\tilde{\boldsymbol{\Phi}}^{*\beta\alpha}_{\boldsymbol{q}}(\boldsymbol{k}',\boldsymbol{k},\omega)-\tilde{\boldsymbol{\Phi}}^{*\beta\alpha}_{-\boldsymbol{q}}(\boldsymbol{k}',\boldsymbol{k},\omega), \quad (52)$$

where

$$\tilde{\boldsymbol{\Phi}}^{\alpha\beta}_{\boldsymbol{q}}(\boldsymbol{k},\boldsymbol{k}',\omega)=(2\pi)^3\delta(\boldsymbol{k}-\boldsymbol{q}-\boldsymbol{k}')V_{\mathrm{s}}G_0(\boldsymbol{k},\omega) \times P^{\alpha\delta}(\boldsymbol{k})[(\boldsymbol{k}\cdot\boldsymbol{n})\delta_{\delta\gamma}+n^{\delta}q^{\gamma}] \times\mathrm{Im}\{G_0(\boldsymbol{k}',\omega)\}\Phi^{\gamma\beta}_0(\boldsymbol{k}'). \quad (53)$$

In $\boldsymbol{k},t$ representation the last equations take the form

$$\hat{\boldsymbol{\Phi}}^{\alpha\beta}_{\boldsymbol{q}}(\boldsymbol{k},\boldsymbol{k}',t)\approx(2\pi)^3\delta(\boldsymbol{k}-\boldsymbol{q}-\boldsymbol{k}')\frac{V_{\mathrm{s}}}{4i\gamma_+}P^{\alpha\delta}(\boldsymbol{k}) \times[(\boldsymbol{k}\cdot\boldsymbol{n})\delta_{\delta\gamma}+n^{\delta}q^{\gamma}]\Phi^{\gamma\beta}_0(\boldsymbol{k}') \times\exp[(i\boldsymbol{k}_+\cdot\boldsymbol{V}_0-\gamma_+)t], \quad (54)$$

where we introduced

$$\boldsymbol{k}_+=\tfrac{1}{2}(\boldsymbol{k}+\boldsymbol{k}'),\quad \gamma(k_+)=\gamma_+. \quad (55)$$

Having in mind the approximation of the linear shear we keep in $\tilde{\boldsymbol{\Phi}}^{\alpha\beta}_{\mathrm{s}}(\boldsymbol{k},\boldsymbol{k}',\omega)$ only terms that are either q-independent or linear in q. Correspondingly, we may present Eq. (54) as

$$\hat{\boldsymbol{\Phi}}^{\alpha\beta}_{\boldsymbol{q}}(\boldsymbol{k},\boldsymbol{k}',t)\approx\frac{\pi^3V_{\mathrm{s}}}{i\gamma_+}\delta(\boldsymbol{k}-\boldsymbol{q}-\boldsymbol{k}')\exp[(i\boldsymbol{k}_+\cdot\boldsymbol{V}_0-\gamma_+)t] \times\Bigg\{P^{\alpha\beta}(\boldsymbol{k}_+)\Bigg[2\boldsymbol{k}_+\cdot\boldsymbol{n}+\boldsymbol{q}\cdot\boldsymbol{n}+(\boldsymbol{k}_+\cdot\boldsymbol{n}) \times(\boldsymbol{q}\cdot\boldsymbol{k})\frac{\partial}{k_+\partial k_+}\Bigg]+2P^{\alpha\gamma}(\boldsymbol{k}_+)n^{\gamma}q^{\delta}P^{\delta\beta}_0(\boldsymbol{k}_+) +(\boldsymbol{k}_+\cdot\boldsymbol{n})\frac{q^{\alpha}k_+^{\beta}-q^{\beta}k_+^{\alpha}}{k_+^2}\Bigg\}\Phi_0(k_+). \quad (56)$$

To compute $\mathcal{F}^{\alpha\beta}_{\mathrm{s}}(\boldsymbol{R},\boldsymbol{R}',t)$ we need to use Fourier transform (17), which involves the integrations $d\boldsymbol{k}\,d\boldsymbol{k}'=d\boldsymbol{k}_+d(\boldsymbol{k}-\boldsymbol{k}')$ and $\exp[i(\boldsymbol{k}\cdot\boldsymbol{R}-\boldsymbol{k}'\cdot\boldsymbol{R}']$. The latter may be presented as

$$\exp[i(\boldsymbol{k}\cdot\boldsymbol{R}-\boldsymbol{k}'\cdot\boldsymbol{R}')]=\exp(i\boldsymbol{k}_+\cdot\boldsymbol{R})\exp[i(\boldsymbol{k}-\boldsymbol{k}')\cdot\boldsymbol{r}_0].$$

Here $\boldsymbol{R}=\boldsymbol{R}-\boldsymbol{R}'$ is the separation between probes and $\boldsymbol{r}_0=\frac{1}{2}(\boldsymbol{R}+\boldsymbol{R}')$ is a mean position of the probes. Now it is customary to introduce a mixed $(\boldsymbol{k}_+,\boldsymbol{r}_0,t)$ representation in which one integrates with respect to $(\boldsymbol{k}-\boldsymbol{k}')$ only:

$$\hat{\mathcal{C}}F^{\alpha\beta}_q(\boldsymbol{k}_+,\boldsymbol{r}_0,t)=\int\frac{d(\boldsymbol{k}-\boldsymbol{k}')}{(2\pi)^3}\hat{\boldsymbol{\Phi}}^{\alpha\beta}_{\boldsymbol{q}}(\boldsymbol{k},\boldsymbol{k}',t) \times\exp[i(\boldsymbol{k}-\boldsymbol{k}')\cdot\boldsymbol{r}_0]. \quad (57)$$

Together with Eqs. (52) and (56) this gives

$$\hat{\mathcal{F}}^{\alpha\beta}_{\mathrm{s}}(\boldsymbol{k},\boldsymbol{r}_0,t)=\frac{1}{2\gamma(k)}\exp\{[i\boldsymbol{k}\cdot\boldsymbol{V}_0-\gamma(k)]t\} \times\Bigg\{P^{\alpha\beta}(\boldsymbol{k})\Bigg[2\boldsymbol{k}\cdot\boldsymbol{V}_{\mathrm{s}}(\boldsymbol{r}_0)+\frac{\partial V^{\gamma}_{\mathrm{s}}(\boldsymbol{r}_0)}{\partial r_0^{\delta}}\frac{k^{\gamma}k^{\delta}\partial}{k\partial k}\Bigg] +P^{\alpha\gamma}(\boldsymbol{k})\Bigg[\frac{\partial V^{\gamma}_{\mathrm{s}}(\boldsymbol{r}_0)}{\partial r^{\delta}}+\frac{\partial V^{\delta}_{\mathrm{s}}(\boldsymbol{r}_0)}{\partial r^{\gamma}}\Bigg]P^{\delta\beta}_0(\boldsymbol{k})\Bigg\} \times\Phi_0(k), \quad (58)$$

where we redefined $\boldsymbol{k}_+\to\boldsymbol{k}$ and used explicit form (22) of $\boldsymbol{V}_{\mathrm{s}}(\boldsymbol{r}_0)$.

Solution (58) contains a term that is proportional to the value of the shear $\boldsymbol{k}$, $\boldsymbol{V}_{\mathrm{s}}(\boldsymbol{r}_0)$ computed at the position $\boldsymbol{r}_0$ between the two probes. This is just a first-order term, representing the first correction to the homogeneous velocity $\boldsymbol{V}_0$ due to the sweeping effect. If we were to compute higher-order sweeping corrections and were to sum them all up, we would find a renormalized sweeping velocity in the exponent: $\boldsymbol{V}_0\to\boldsymbol{V}_0+\boldsymbol{V}_{\mathrm{s}}(\boldsymbol{r}_0)$. Thus instead of Eq. (58) one writes

$$\hat{\mathcal{F}}^{\alpha\beta}_{\mathrm{s}}(\boldsymbol{k},\boldsymbol{r}_0,t)=\frac{1}{2\gamma(k)}\exp\{i\boldsymbol{k}\cdot[\boldsymbol{V}_0+\boldsymbol{V}_{\mathrm{s}}(\boldsymbol{r}_0)]t-\gamma(k)t\} \times\Bigg[\frac{\partial V^{\gamma}_{\mathrm{s}}(\boldsymbol{r}_0)}{\partial r^{\delta}}+\frac{\partial V^{\delta}_{\mathrm{s}}(\boldsymbol{r}_0)}{\partial r^{\gamma}}\Bigg]\Bigg[P^{\alpha\beta}(\boldsymbol{k})k^{\gamma}k^{\delta}\frac{\partial\Phi_0(k)}{\partial^2k} +P^{\alpha\gamma}(\boldsymbol{k})P^{\delta\beta}(\boldsymbol{k})\Phi_0(k)\Bigg]. \quad (59)$$

We should comment at this point that the calculation resulted in an intuitively pleasing rule: effective Taylor wind should be taken as the mean wind at the point midway between the two probes. Also, we see that the magnitude of the shear-induced part is proportional to the shear midway between the probes. Of course, this simple rule is a result of the assumption of *linear* shear. Nevertheless, as long as the shear profile is not too nonlinear on the scale of the separation between the two probes, this simple rule can be taken as a rule of thumb for experimental applications.

Finally, we remember that the space homogeneous part of the wind $\boldsymbol{V}_0$ has a fluctuating component, $\boldsymbol{V}_0=\overline{\boldsymbol{V}_0}+\boldsymbol{V}_{\mathrm{T}}$. One has to average therefore the result using the Gaussian distribution $\mathcal{P}(\boldsymbol{V}_{\mathrm{T}})$. The final answer in analogy with Eq. (36) reads

$$\hat{\mathcal{F}}_s^{\alpha\beta}(\boldsymbol{k},\boldsymbol{r}_0,t)=\mathcal{F}_s^{\alpha\beta}(\boldsymbol{k},\boldsymbol{r}_0)\exp\{i\boldsymbol{k}\cdot[\overline{\boldsymbol{V}}_0+\boldsymbol{V}_s(\boldsymbol{r}_0)]t - \gamma(k)t-2(v_T kt)^2\},$$

$$\mathcal{F}_s^{\alpha\beta}(\boldsymbol{k},\boldsymbol{r}_0)=\frac{\omega_s(\boldsymbol{r}_0)}{2\gamma(k)}\left[2P^{\alpha\beta}(\boldsymbol{k})(\boldsymbol{k}\cdot\boldsymbol{n})(\boldsymbol{k}\cdot\boldsymbol{m})\frac{\partial\Phi_0(k)}{\partial^2 k} + P^{\alpha\gamma}(\boldsymbol{k})(n^\gamma m^\delta+n^\delta m^\gamma)P^{\delta\beta}(\boldsymbol{k})\Phi_0(k)\right], \tag{60}$$

where in agreement with Eq. (22) we introduced a ''shear frequency'' $\omega_s(\boldsymbol{r})$ according to

$$\frac{\partial V_s^\alpha(\boldsymbol{r}_0)}{\partial r^\beta}\equiv\omega_s(\boldsymbol{r}_0)n^\alpha m^\beta. \tag{61}$$

Examining Eq. (60) we see that the scaling exponent expected for $\mathcal{F}_s^{\alpha\beta}(\boldsymbol{k},\boldsymbol{r}_0)$ is determined by the scaling of $\Phi_0(\boldsymbol{k})$ and $\gamma(k)$ with the choices specified in Eqs. (24) and (29) $\mathcal{F}_s^{\alpha\beta}(\boldsymbol{k},\boldsymbol{r}_0)\propto k^{-13/3}$, or $R^{4/3}$ for the second-order structure function. This is consistent with the expected scaling in the anisotropic sector characterized by $j=2$, see [3] for more details.

Note that in the case linear shear the frequency $\omega_s(\boldsymbol{r})$ is $\boldsymbol{r}$ independent. Similarly to Eqs. (38) and (39) one computes the shear-induced additions of $S_s^{\alpha\beta}(\boldsymbol{R})$ and $T_s^{\alpha\beta}(t)$ to the usual and Taylor-computed structure functions $S^{\alpha\beta}(\boldsymbol{R})$ and $T^{\alpha\beta}(t)$:

$$S_s^{\alpha\beta}(\boldsymbol{R})=\int\frac{d\boldsymbol{k}}{4\pi^3}\mathcal{F}_s^{\alpha\beta}(\boldsymbol{k})\{1-\cos(\boldsymbol{k}\cdot\boldsymbol{R})\}, \tag{62}$$

$$T_s^{\alpha\beta}(t)=\int\frac{d\boldsymbol{k}}{4\pi^3}\mathcal{F}_s^{\alpha\beta}(\boldsymbol{k})\{1-\exp[-2(v_T kt)^2-\gamma(k)|t|] \times\cos\{\boldsymbol{k}\cdot[\overline{\boldsymbol{V}}_0+\boldsymbol{V}_s(\boldsymbol{r}_0)]t\}\}.$$

In experimental measurements we can isolate the shear-induced contribution at the expense of the isotropic contribution by considering a mixed, transverse-longitudinal structure function, taking the separation $\boldsymbol{R}$ along the wind $\boldsymbol{R}_{/\!/}=\boldsymbol{n}(\boldsymbol{R}\cdot\boldsymbol{n})$. For example,

$$S_s^{t/\!/}(R)\equiv S_s^{\alpha\beta}(\boldsymbol{R}_{/\!/})m^\alpha n^\beta,\quad T_s^{t/\!/}(t)\equiv T_s^{\alpha\beta}(t)m^\alpha n^\beta. \tag{63}$$

These functions may be obtained from equations similar to Eq. (62) with the replacement

$$\mathcal{F}_s^{\alpha\beta}(\boldsymbol{k})\to\mathcal{F}_s^{t/\!/}\equiv\mathcal{F}_s^{\alpha\beta}(\boldsymbol{k})m^\alpha n^\beta \tag{64}$$

$$=\frac{\omega_s}{\gamma(k)}\left\{-\frac{(\boldsymbol{k}\cdot\boldsymbol{n})^2(\boldsymbol{k}\cdot\boldsymbol{m})^2}{k^2}\frac{d\Phi_0(k)}{dk^2} + \frac{1}{2}\left[1-\frac{(\boldsymbol{k}\cdot\boldsymbol{n})^2}{k^2}\right]\left[1-\frac{(\boldsymbol{k}\cdot\boldsymbol{m})^2}{k^2}\right]\Phi_0(k)\right\}. \tag{65}$$

Integrating this over ϕ, the azimuthal angle of $\boldsymbol{k}$ around the direction of $\boldsymbol{n}$, one has

$$\int_0^{2\pi}\delta\phi\,\mathcal{F}_s^{t/\!/}=\frac{\pi\omega_s\sin^2\theta}{\gamma(k)} \times\left\{-2\frac{d\,\Phi_0(k)}{d\,k^2}\cos^2\theta+\Phi_0(k)(1+\cos^2\theta)\right\}, \tag{66}$$

where $\cos\theta=\boldsymbol{n}\cdot\boldsymbol{k}/k$. Having this in mind and performing in Eq. (62) the θ integration we end up with

$$S_s^{t/\!/}(\boldsymbol{R})=\frac{\omega_s}{5\pi^2}\int_0^\infty\frac{k^2dk}{\gamma(k)}\left\{\Phi_0(k)[1-\Psi_s^{t/\!/}(kr)] - \frac{k^2}{3}\frac{d\Phi_0(k)}{d\,k^2}[1-\overline{\Psi}_s^{t/\!/}(kr)]\right\}, \tag{67}$$

$$T_s^{t/\!/}(t)=\frac{\omega_s}{5\pi^2}\int_0^\infty\frac{k^2dk}{\gamma(k)}\left\{\Phi_0(k)\{1-\Psi_s^{t/\!/}(kV_{ad}t) \times\exp[-2(v_T kt)^2-\gamma(k)t]\}-\frac{k^2}{3}\frac{d\Phi_0(k)}{d\,k^2} \times\{1-\overline{\Psi}_s^{t/\!/}(kV_{ad}t)\exp[-2(v_T kt)^2-\gamma(k)t]\}\right\}, \tag{68}$$

$$\Psi_s^{t/\!/}(x)=5\left[\frac{6-x^2}{x^4}\cos x+3\frac{x^2-2}{x^5}\sin x\right] \simeq 1-\frac{5x^2}{42}, \tag{69}$$

$$\overline{\Psi}_s^{t/\!/}(x)=15\left[\frac{12-x^2}{x^4}\cos x+\frac{5x^2-12}{x^5}\sin x\right]\simeq 1-\frac{5x^2}{14}.$$

Formally expansion of $\Psi_s^{t/\!/}(x)$ and $\overline{\Psi}_s^{t/\!/}(x)$ at small x begin with $1/x^4$ terms, but due to double cancellation it actually starts from 1. We analyzed numerically Eqs. (67)–(69) in the following subsection.

B. Discussion of the case of shear

The first difference between Eqs. (67)–(69) for the anisotropic contribution to the structure functions $S_s^{t/\!/}$ and $T_s^{t/\!/}$ and the corresponding structure functions $S_0^{\alpha\beta}$ and $T_0^{\alpha\beta}$ is in their scaling behavior. In integrals (41)–(44) for $S_0^{\alpha\beta},T_0^{\alpha\beta}$ the function $\Phi_0(k)\propto k^{-11/3}$. These integrals converge, and the main contribution comes from the region $kR\sim 1$. Both quantities scale according to $S_0^{\alpha\beta}(R)\propto R^{2/3}$ and $T_0^{\alpha\beta}(R)\propto R^{2/3}$ in the limit $R/L\to 0$, as expected. In contrast to that, the integrands in Eqs. (67)–(69) have an additional factor $\gamma(k)\propto k^{2/3}$ in the denominator. This changes the scaling behavior to $S_s^{t/\!/}(R)\propto R^{4/3}, T_s^{t/\!/}(R)\propto R^{4/3}$. The second difference is in the rates of the convergence. The integrals for $S_0^{\alpha\beta}$ and $T_0^{\alpha\beta}$ behave in the region of $kL\ll 1$ like $\int_0 k^{1/3}dk$ while the integrals for $S_s^{t/\!/}$ and $T_s^{t/\!/}$ behave in the region of small k like $\int_0 k^{-1/3}dk$. One sees that the latter integrands have an inte-

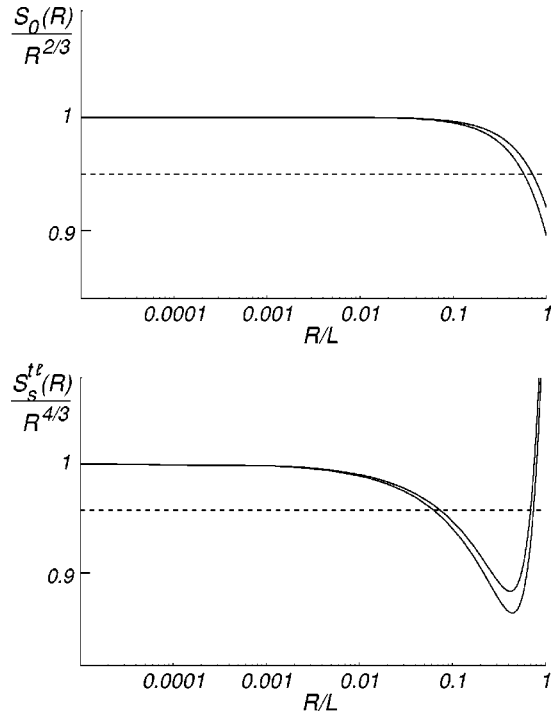

FIG. 4. A log-log plot of the ratio of $S_0(R)/R^{2/3}$ vs R/L (top panel) and $S_s^{t\ell}(R)/R^{4/3}$ (bottom panel) vs R/L. Different lines correspond to different choices (29) and (30) of the power spectrum $\Phi_0(k)$. Dashed line denotes level 0.95.

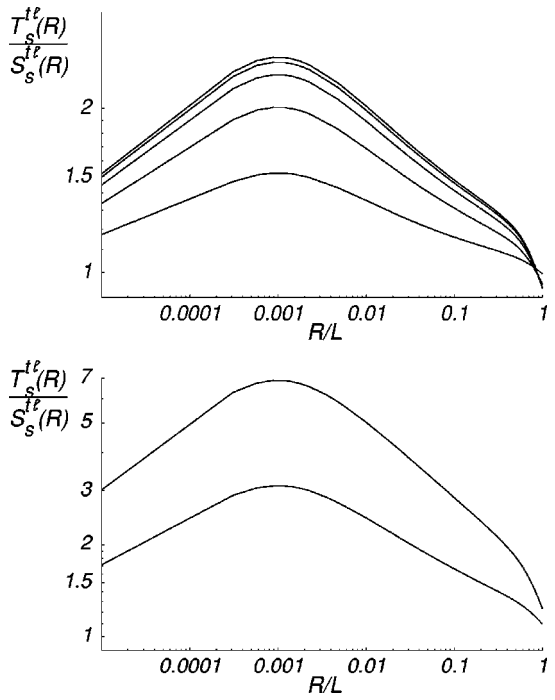

FIG. 5. On the top panel, a log-log plot of the ratios $T_s^{t\ell}(R/V_{ad})/S_s^{t\ell}(R)$ vs R/L for $C=0.25$ and different values of $q=10$ (upper line); $q=1$, 0.5, and 0.25 from top to bottom and $q=0.1$, the bottom line. The bottom panel represents the ratios for $C=1$. The top line corresponds to $q=10$, the bottom line corresponds to $-q=0.1$.

grable singularity. The contribution of the nonuniversal energy containing region $kL\sim 1$ is much more pronounced than in the corresponding integral $\int_0 k^{1/3}dk$. As a consequence one needs to consider much smaller values of R/L to see the asymptotic scaling of the functions $S_s^{t\ell}$ and $T_s^{t\ell}$ compared to the case of $S_0^{\alpha\beta}$ and $T_0^{\alpha\beta}$. This is illustrated in Fig. 4. The top panel shows log-log plots of $S_0(R)/R^{2/3}$ vs R/L for choices (29) and (30) of cutoff functions Φ_0. The two lines almost coincide and reach a level of 0.95 at $R\simeq L/3$. The bottom panel exhibits the corresponding log-log plots of $S_s^{t\ell}(R)/R^{4/3}$ vs R/L. The plots reach the level 0.95 at much smaller R values (about $R\simeq L/10$), as expected. However, the two plots are significantly different only when there is no scaling behavior (for $R>L/3$). We thus propose that our main findings are independent of the choice of the crossover behavior of the power spectrum $\Phi_0(k)$ (within reason).

As mentioned above, for small mean winds the Taylor method is problematic for large values of R but it improves for smaller values. Therefore, the significantly more pronounced contribution of the large scale eddies for the shear-induced part of the structure functions (in comparison with the isotropical one) has to lead to larger deviations of the Taylor surrogate $T_s^{t\ell}(R)$ from the directly measured structure function $S_s^{t\ell}(R)$. This is illustrated by the log-log plots of the ratio $T_s^{t\ell}(R)/S_s^{t\ell}(R)$ vs. R/L in Fig. 5. The top panel represents this ratio for $c=0.25$ and for values of the parameter d ranging between $d=0.1$ (lower line), $d=0.25,0.5,1$, and $d=\infty$ (upper line). In contrast to the isotropic case we have here two regimes, one with negative apparent correction to the scaling exponent (in the region $10^{-3}L<R<0.3L$) and a second with a positive correction (for $R<10^{-3}L$). The largest possible corrections are obtained in the absence of the mean wind ($d=\infty$), reaching ± 0.13. For $d=0.25$ the corrections are about ± 0.1 and for $d=0.1$ they are about ± 0.06. The bottom panel shows the ratio for $c=1$ and $d=\infty$ (upper line) and $d=0.1$ (lower line). The corrections to the apparent scaling exponents are ± 0.21 and ± 0.15, respectively. The conclusion is that in the absence of the mean wind ($d=\infty$) one has to be weary of using the Taylor surrogate instead of direct measurements in space. If the mean wind is relatively large (say, $d<0.1$, as is quite common) the expected error in the scaling exponent is about 0.1. This is definitely a large error but it is substantially smaller than the difference between the isotropic and the shear-induced exponents for the second-order structure functions (2/3).

V. SUMMARY AND DISCUSSION

In this paper we presented an exactly soluble model of an advected field whose fluctuations are chosen to mimic as closely as possible those of turbulence with K41 spectra. The aim was to assess the accuracy of the Taylor surrogate structure function by solving exactly for the space-dependent and the time-dependent second-order structure functions and to compare between them. Clearly, the most important consideration is the decay time of correlations of size R compared to the rate of sweeping across R. The parameter C in our model determines the ratio of the turnover time to the decay time, and is free in our model.

The main results of the analysis are as follows.

(a) For data extracted from a single probe in isotropic flows the error introduced by the Taylor method is systematic, always leading to an overestimate in the scaling expo-

nent of the second-order structure function. This is in agreement with the conclusions of Sreenivsan and co-workers who studied this issue experimentally [14,15].

(b) The error in the isotropic scaling exponent, which is introduced by the Taylor method, is typically small, reaching 0.01 in the most adverse situation.

(c) The rms velocity is an important contribution to the effective wind, and should not be left out. Equation (47) is a simple recipe that can be followed, with b chosen to minimize the errors. We found that our model yields the smallest errors with $b \approx 3.1$.

(d) For data extracted from two probes in anisotropic fields the best rule of thumb is to use the mean velocity and mean rms of the two probes. The best value of b for the model treated above is $b = 3.8$.

(e) The errors introduced by the Taylor method in anisotropic fields are considerably larger than those found in isotropic flows. In the most adverse situation errors in the scaling exponents can reach 0.15. Worse, they are not systematic, tending from positive errors for smaller scales to negative errors for larger scales.

(f) Nevertheless, the errors are significantly smaller than the difference between the exponents in the different sectors of the symmetry group. Thus, the Taylor approach can be used (with care) to extract the universal exponents characterizing the different sectors. An example of such an approach can be found in [13].

Even though these results are found on the basis of a simple model, there are aspects that appear relatively model independent. The source of error in the Taylor method is the finite lifetime of the fluctuations and the parameter C that appears in the model, the ratio of this to the sweeping time is going to appear in a similar fashion in any other model or experiment. The relative improvement of the Taylor estimates with decreasing scales is also model independent. The need for a ''unit fixer'' like b is generic as well, especially when we mix spatial and temporal distances, as is the case with data measured by two probes. We thus hope that the analysis presented above would be of some use for assessing experimental data as long as the Taylor surrogates have not been replaced by direct methods of measurements.

ACKNOWLEDGMENTS

This work has been supported in part by the Israel Science Foundation administered by the Israel Academy of Sciences and Humanities, the German-Israeli Foundation, the European Commission under the TMR program, the Henri Gutwirth Fund for Research, and the Naftali and Anna Backenroth-Bronicki Fund for Research in Chaos and Complexity.

[1] G.I. Taylor, Proc. R. Soc. London, Ser. A **164**, 476 (1938).
[2] I. Arad, B. Dhruva, S. Kurien, V.S. L'vov, I. Procaccia, and K.R. Sreenivasan, Phys. Rev. Lett. **81**, 5330 (1998).
[3] I. Arad, V.S. L'vov, and I. Procaccia, Phys. Rev. E **59**, 6753 (1999).
[4] C.F. von Weizäcker, Z. Phys. **124**, 614 (1948).
[5] Y. Ogura, J. Meteorol. Soc. Jpn. **31**, 355 (1953).
[6] F. Gifford, Jr., J. Met. **13**, 289 (1956).
[7] See also, A.S. Monin and A.M. Yaglom, *Statistical Fluid Mechanics*, (MIT, Cambridge, 1975), Vol. 2.
[8] V.S. L'vov, Phys. Rev. Lett. **67**, 687 (1991).
[9] J.-F. Pinton, and R. Labbé, J. Phys. II **4**, 1461 (1994).
[10] K.R. Sreenivasan and B. Dhruva, Prog. Theor. Phys. Suppl. **130**, 103 (1998).
[11] A. Praskovsky and S. Oncley, Phys. Fluids **6**, 2886 (1994).
[12] D.C. Leslie, *Developments in the Theory of Turbulence* (Clarendon, Oxford, 1973).
[13] S. Kurien, V.S. L'vov, I. Procaccia, and K.R. Sreenivasan (unpublished).
[14] B. Dhruva and K. R. Sreenivasan (unpublished).
[15] L. Zubair, Ph.D. dissertation, Yale University, 1993.